Surface Structure of $SrTiO_3(100)$-$(\sqrt{5} \times \sqrt{5})$-$R26.6°$

T. Kubo and H. Nozoye*

National Institute of Materials and Chemical Research, 1-1 Higashi, Tsukuba, Ibaraki 305-8565, Japan

(Received 3 August 2000)

Atomic and electronic structures of the $SrTiO_3(100)$-$(\sqrt{5} \times \sqrt{5})$-$R26.6°$ surface are studied by using scanning tunneling microscopy (STM) and noncontact atomic force microscopy (NC-AFM). Instead of the well established oxygen vacancy model, it is found that a structural model, consisting of an ordered Sr adatom at the oxygen fourfold site of a TiO_2 terminated layer, can explain the experimental results very well. We theoretically simulate the model cluster with the first-principles total-energy calculation. Calculated density of states and images for STM and NC-AFM are in good agreement with the experimental results.

DOI: 10.1103/PhysRevLett.86.1801 PACS numbers: 68.35.Bs, 68.37.Ef, 68.37.Ps, 71.20.Ps

Surfaces of metal oxides serve very important roles in varieties of applications. However, surface sciences of metal oxides have not been developed so much compared to those of metals and semiconductors, because the surfaces of metal oxides are defective in nature and also metal oxides are usually insulators and modern surface analytical tools as electron spectroscopy are not fully applicable to these materials [1–3]. Scanning tunneling microscopy (STM), which has revolutionized the field of surface science, is not applicable to insulators. Furthermore, as STM image is related to the shape of the wave functions near the Fermi level [4], atoms which do not have the local density of states near the Fermi level are generally invisible even on the conductive materials. Noncontact atomic force microscopy (NC-AFM) is a powerful tool and has a possibility to give a new aspect to surface science of metal oxides because it has a potential to observe atomic images even for the surface of nonconductive materials [5–8].

Strontium titanate ($SrTiO_3$) is one of the perovskite oxides and has been of interest in many aspects including catalytic activities, dielectric properties, ferroelectric properties, and a lattice-matched substrate for high-T_c oxide superconductors. Many structures related to the $SrTiO_3(100)$ surface have been reported, e.g., rowlike structures [9], 1×1 [10], 2×1 [10], $c(4 \times 2)$ [10], $c(6 \times 2)$ [10], and $(\sqrt{5} \times \sqrt{5})$-$R26.6°$ [11,12]. As many kinds of metal oxides form a wide range of oxygen deficiency intermediate phases [3], it is generally believed that the reconstruction of metal oxide surface is related to an ordered oxygen vacancy type defect. In the case of the $(\sqrt{5} \times \sqrt{5})$-$R26.6°$ reconstruction, the defects are proposed to be a $\square$-Ti^{3+}-O ($\square$: oxygen vacancy) complex, which was determined by STM [11]. However, several theoretical results are inconsistent with STM images [13,14]. In this study, the $SrTiO_3(100)$-$(\sqrt{5} \times \sqrt{5})$-$R26.6°$ surface was observed by use of NC-AFM as well as STM, and we propose a Sr adatom model, which is supported by *ab initio* calculations, instead of the well established oxygen vacancy model.

Experiments were carried out in an ultrahigh vacuum NC-AFM (JEOL model JAFM-4400) with a base pressure of $\leq 1.4 \times 10^{-8}$ Pa. Cone-shaped silicon cantilevers with $f_0 = 140$–290 kHz and $k = 4$–14 N/m (Silicon-MDT Ltd.), which were highly doped with B (0.002 Ω cm) and coated with W_2C (25 nm thick, 30 $\mu\Omega$ cm), were used for NC-AFM measurements. NC-AFM measurements were performed by the constant force condition. Tips used for STM measurements were the same cantilevers or made of a tungsten wire, 0.3 mm in diameter, by electrochemical etching in 2N KOH solution. STM measurements were performed either in the constant current condition or the spectroscopic sequence.

A $SrTiO_3(100)$ substrate of $7 \times 1 \times 0.5$ mm^3 (Nakazumi Crystal Co., Japan) was first treated with a buffered NH_4F-HF (BHF) solution (pH = 4.5 and NH_4F concentration of 10 M) for 10 min [15]. The sample was directly mounted on a silicon heater. Vacuum pressure during annealing did not exceed 5×10^{-7} Pa. Temperature was measured with an optical pyrometer. TiO_2 terminated and $(\sqrt{5} \times \sqrt{5})$-$R26.6°$ surfaces of $SrTiO_3(100)$ were obtained by annealing at 800 and 1200 °C, respectively [11,15].

The calculations were performed by an *ab initio* ultrasoft pseudopotential technique with a plane-wave basis. In this method, valence electron wave functions were obtained by minimizing the Kohn-Sham total-energy function [16]. The exchange correlation potential was treated with the generalized gradient approximation (GGA) [17]. The self-consistent ultrasoft pseudopotential proposed by Vanderbilt [18] was used for electron-ion interaction. A plane-wave cutoff of 260 eV and Monkhorst-Pack mesh [19] of (2,2,1) were used. The TiO_2-terminated 1×1 and the Sr adatom $(\sqrt{5} \times \sqrt{5})$-$R26.6°$ surfaces of $SrTiO_3(100)$ were modeled by periodic slabs. The periodic slabs consisted of seven atomic layers of SrO and TiO_2 stacked alternately, which were isolated by $3 \times a_{STO}$ width of vacuum regions. For the Sr adatom model, a Sr atom was placed on a TiO_2 terminated $(\sqrt{5} \times \sqrt{5})$ unit lattice. Atoms at central three layers were fixed at the bulk position; on the other hand, all other atoms were geometry optimized. The criteria of energy change per atom, root mean square (rms) displacement of atoms, and rms force on each atom were

0.001 eV, 0.01 Å, and 0.5 eV/Å, respectively. Gaussian smearing of 0.2 eV was used.

Figure 1a shows an STM image of a 50 × 50 nm^2 region of $SrTiO_3$(100) after heating at 1200 °C. The surface is composed of two orientations of $(\sqrt{5} \times \sqrt{5})$-$R26.6°$ domains and large bright particles, which are related to Sr or SrO clusters [12] and are mainly observed at domain boundaries and step edges. The number and the size of the particles decrease with extended annealing and, when the size is small, these are always located at bright lattice points (not shown). Our STM images and the behavior of the large particles are quite similar to the reported results [11,12]. For this reconstruction, the □-Ti^{3+}-O model (the terminated surface is TiO_2 and the observed spots are related to the oxygen vacancy) was proposed by Tanaka *et al.* [11]. However, several theoretical works predicted that the bright spots of STM images, located at the oxygen vacancy, should be split into two spots, because the defect surface states were mostly derived from the nearest two Ti 3*d* orbitals [13,14]. In contrast, the shape of the bright spots of the STM images was always observed to be a round shape [11,12]. Moreover, it is unaccountable why other surface atoms are invisible in STM measurements.

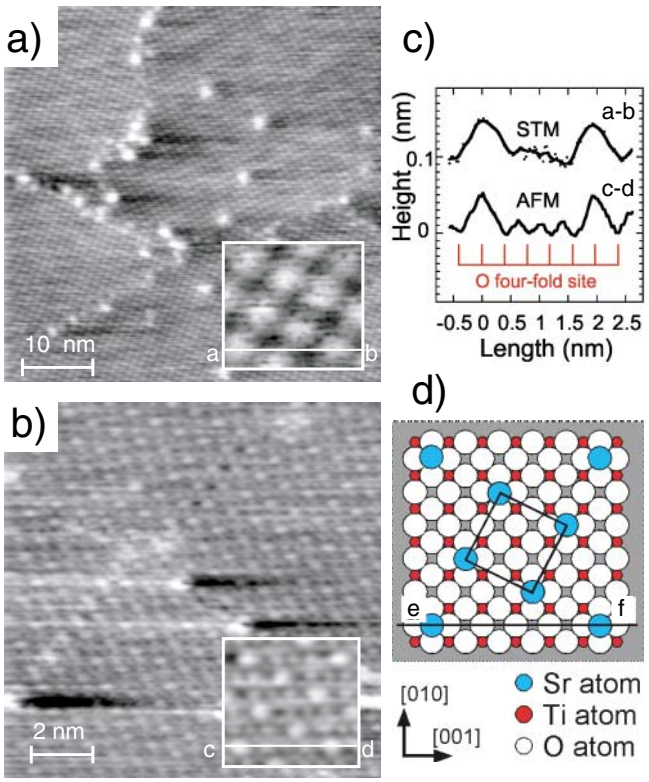

FIG. 1 (color). (a) STM ($V = +0.65$ V, $I = 0.11$ nA, and 50 × 50 nm^2) and (b) NC-AFM ($V = -1.49$ V and 12 × 12 nm^2) images of $SrTiO_3$(100) after heating at 1200 °C for several seconds. (c) The vertical profiles along the lines *a*-*b* and *c*-*d*. (d) A proposed model of the $SrTiO_3$(100)-$(\sqrt{5} \times \sqrt{5})$-$R26.6°$ surface reconstruction; a line *e*-*f* corresponds to the lines *a*-*b* and *c*-*d* in (a) and (b), respectively.

In order to clarify the structure of the surface reconstruction, NC-AFM measurements were performed as shown in Fig. 1b. In addition to the bright spots of $(\sqrt{5} \times \sqrt{5})$-$R26.6°$ lattice, four dark spots were clearly observed inside the lattice. Figure 1c shows vertical profiles along the lines *a*-*b* and *c*-*d*. The size of the bright spots for the NC-AFM measurements (~0.3 nm) was always smaller than that for the STM measurements (~0.5 nm). In order to exclude the effects of probe shape, STM measurements using the same NC-AFM cantilever were performed. However, STM images were the same as those observed by using a W tip.

Many previous results show that NC-AFM images are determined well by the cantilever-sample interaction and protrusions represent surface atomic positions unless specific interaction as chemical bonding interaction is dominant [20,21]. In fact, Yokoyama *et al.* reported that, when an Ag-coated cantilever was used, NC-AFM images for Si(111)-$(\sqrt{3} \times \sqrt{3})$-Ag did not depend on cantilever-sample distance and showed true topography [20]. On the other hand, Minobe *et al.* did not observe true atomic protrusion, when a silicon cantilever was used, because of chemical bonding interaction between the dangling bond of a tip apex Si atom and the surface [22]. In the present study using a less reactive W_2C coated cantilever, NC-AFM images did not change with the cantilever-sample distance. It is considered that chemical bonding interaction is not dominant and the NC-AFM image reflects a surface corrugation in our experimental conditions; i.e., the bright and the dark spots are related to a surface atomic position and a hollow position, respectively. It is noted that the dark spots are aligned along the [001] and [010] directions, which are shown in the inset of Fig. 1b, suggesting that the surface layer must be TiO_2 plane and the dark spot is related to the oxygen fourfold hollow site. If the surface layer were SrO plane, the dark spots would be aligned along the [011] and [01$\bar{1}$] directions from our calculations (not shown). The bright spots are located on the oxygen fourfold site, as shown in Fig. 1c, where a Sr atom is considered to be located compared with the bulk crystal structure. We propose a Sr adatom model in which Sr adatoms are assumed to be located on the oxygen fourfold site of the TiO_2 terminated layer forming a $(\sqrt{5} \times \sqrt{5})$-$R26.6°$ lattice as shown in Fig. 1d. This model agrees with the fact that the small particles, which are probably Sr-related clusters, are always located with footing at the Sr adatom site.

Figure 2 shows the optimized structure of the Sr adatom $(\sqrt{5} \times \sqrt{5})$-$R26.6°$ model determined by the first-principles total-energy calculations. A Sr adatom attracts surrounding first layer O atoms by 0.177 Å; in contrast, a Sr adatom and first layer Ti atoms repel each other. As a result, we can see large displacement (−21%) between the Sr adatom layer and the first TiO_2 layer. On the other hand, the changes of the interlayer spacing between the first and the second layers, and the second and the third layers are −0.54% and +1.23%, respectively, which are substantially small compared with those for the TiO_2

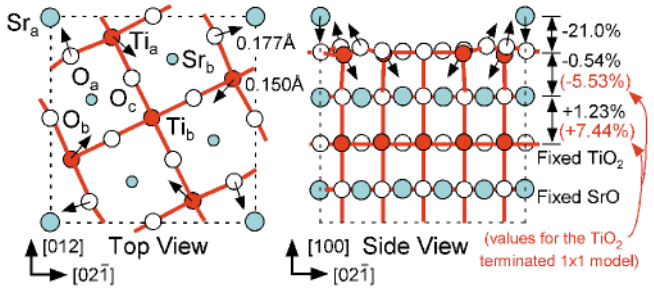

FIG. 2 (color). The optimized structure of Sr adatom $(\sqrt{5} \times \sqrt{5})$-$R26.6°$ model. The values show the atomic displacement and relative interlayer spacing to that for the bulk $SrTiO_3$ value ($a_{STO}/2 = 0.19525$ Å).

terminated 1×1 model of -5.53% and $+7.44\%$, respectively. Detailed atomic displacements are summarized in Table I. For the Sr adatom $(\sqrt{5} \times \sqrt{5})$-$R26.6°$ model, we can see large rumpling for the first layer TiO_2 and small rumpling for the second layer SrO, compared with that of the TiO_2 terminated 1×1 model. The calculation indicates that the Sr adatom causes a large distortion in the first TiO_2 layer but less distortion in the deeper layers in order to lower the total energy.

The calculated density of states (DOS) of the structural models optimized for TiO_2 terminated 1×1 and Sr adatom $(\sqrt{5} \times \sqrt{5})$-$R26.6°$ are shown in Fig. 3a. The electronic energy band gap (E_g) for the TiO_2-terminated 1×1 model was estimated to be 1.31 eV. This value seems to be consistent with the published results of 1.83 eV reported by Li *et al.* [23] and 1.13 eV reported by Padilla and Vanderbilt [24]. On the other hand, E_g for the Sr adatom $(\sqrt{5} \times \sqrt{5})$-$R26.6°$ model was estimated to be 2.32 eV, which was larger than that of the TiO_2 terminated 1×1 model. Additionally, the conduction bands are remarkably lowered and they cross the Fermi level because the Sr adatoms donate its outermost $5s$ electron to the surface and partially fill the conduction band of the TiO_2 terminated layer. In order to get insight in the surface electronic states, dI/dV-V properties were measured for each surface as shown in Fig. 3b. The electronic energy band gap for the $(\sqrt{5} \times \sqrt{5})$-$R26.6°$ surface is relatively larger than that for the TiO_2 terminated surface. Remarkably, the shape of DOS for the TiO_2 surface is symmetric with respect to the Fermi level; on the other hand, that for the $(\sqrt{5} \times \sqrt{5})$-$R26.6°$ surface shows asymmetric property. As the calculated Fermi level for the TiO_2 terminated 1×1 model is located in the midgap, the dI/dV-V curve for the TiO_2 terminated surface should be semiconducting. On the other hand, in the case of the Sr adatom $(\sqrt{5} \times \sqrt{5})$-$R26.6°$ model, the calculated Fermi level is located at the bottom of the conduction band. The dI/dV-V curve with a positive sample bias voltage (tunneling of electron from the STM tip into unoccupied conduction band in the sample) starts to increase immediately from zero bias voltage. For a negative sample bias voltage (tunneling of electron from occupied states in the sample, which are located under the gap, into the STM tip), the curve does not increase immediately.

TABLE I. Vertical atomic displacements relative to average positions of the corresponding planes for the TiO_2 terminated 1×1 and the Sr adatom $(\sqrt{5} \times \sqrt{5})$-$R26.6°$ models. The values are expressed in Å.

Layer	TiO_2 terminated 1×1		Sr adatom $(\sqrt{5} \times \sqrt{5})$-$R26.6°$	
1	O	+0.038	O_a	+0.152
			O_b	−0.010
			O_c	−0.006
	Ti	−0.075	Ti_a	−0.117
			Ti_b	−0.094
2	O	−0.078	O_a	−0.001
			O_b	+0.010
	Sr	+0.078	Sr_a	+0.013
			Sr_b	−0.005

NC-AFM images with highest lateral resolution originate with a short range repulsive cantilever-sample interaction rather than a long range attractive interaction [25], such as van der Waals interaction and local electrostatic interaction. Local electrostatic interaction between the sample and a cantilever, which should be present for ionic materials such as this, was estimated by using *ab initio* calculations (not shown). The results indicated that the atomic resolved image could not be obtained by electrostatic interaction, because calculated electrostatic potential was geometrically broad and considerably screened. Since the repulsive interaction is due to the Pauli repulsion which originates from the overlapping of the wave functions, it is considered that the NC-AFM image is related to the total charge density of states. On the other hand, the STM image is related to the local density of states near the Fermi level [4]. In order to analyze the STM and NC-AFM images, the orbital density and its shapes of the states near the Fermi level (369th to 374th bands) and of the occupied total density of states (1st to 370th bands) were calculated

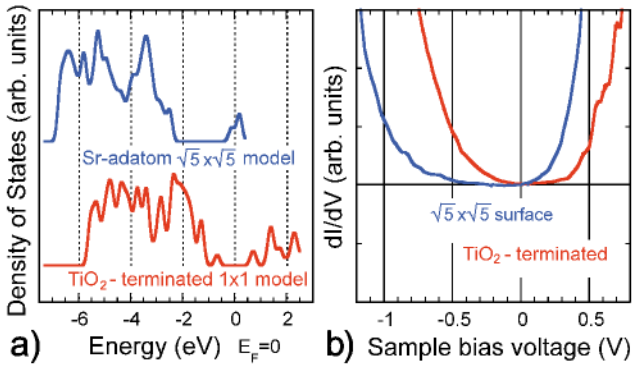

FIG. 3 (color). (a) Calculated density of states for the TiO_2 terminated 1×1 and the Sr adatom $(\sqrt{5} \times \sqrt{5})$-$R26.6°$ models. (b) dI/dV-V properties, after smoothing, for the TiO_2 terminated and the $(\sqrt{5} \times \sqrt{5})$-$R26.6°$ $SrTiO_3(100)$ surfaces.

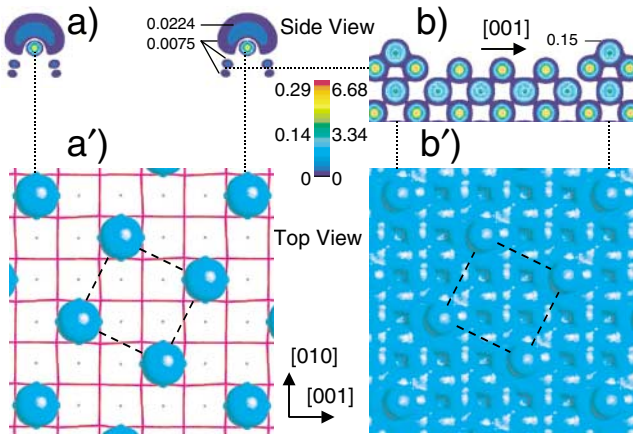

FIG. 4 (color). (a) Calculated density contour and (a′) equidensity surface (blue surface represents the density level of 0.02 $e/\text{Å}^3$) of the wave functions near the Fermi level (371st and 372nd bands). (b) Calculated electron density contour and (b′) equielectron density surface (blue surface represents the density level of 0.1 $e/\text{Å}^3$) of the occupied total wave functions (1st to 370th bands). The cut planes of (a) and (b) are perpendicular to the surface and along the [001] direction including the Sr adatom. The equielectron density surfaces are artificially illuminated from the upper right for the sake of understanding.

for the Sr adatom $(\sqrt{5} \times \sqrt{5})$-$R26.6°$ model. Large surface states (371st and 372nd bands), which were localized at the Sr adatoms and protruded to vacuum, are shown in Figs. 4a and 4a′. Other wave functions near the Fermi level, which were localized around the Ti atoms, were considerably small in size (not shown) and these have little contributions to the STM images. It is noted that the sample bias voltage dependent (-3 – $+3$ V) changes in the STM images were not observed except for a decrease in contrast. Because of the large surface state orbital and the size of the apex of the W tip, it is difficult to get information about the deeper TiO_2 layer. As the Fermi level was located between the 370th and 371st bands, the displayed orbitals were originally unoccupied orbitals. However, the 371st and 372nd bands were only 0.12 and 0.18 eV higher than the Fermi level, respectively. Taking their bandwidths into consideration, these bands cross the Fermi level. On the other hand, the shape of the occupied total density of states, as shown in Figs. 4b and 4b′, which is almost the same as the ball model shown in Fig. 1d, is also consistent with the NC-AFM results.

Finally, we also calculated the $(\sqrt{5} \times \sqrt{5})$-$R26.6°$ □-Ti^{3+}-O model. The images of NC-AFM could not be explained by the occupied total density of states for this model. Furthermore, most of the wave functions near the Fermi level were derived from the surface Ti $3d$ orbitals. Although several wave functions were localized around the O vacancy, the shape of which was oval and the size of all wave functions near the Fermi level were almost the same. The results strongly suggest that the shape of the $(\sqrt{5} \times \sqrt{5})$ spots anticipated by the □-Ti^{3+}-O model must be oval and other Ti atoms should be visible in STM measurements. It is concluded that the □-Ti^{3+}-O model is unacceptable.

In conclusion, we investigated the $SrTiO_3(100)$-$(\sqrt{5} \times \sqrt{5})$-$R26.6°$ surface by use of NC-AFM and STM. It is found that a structural model consisted of an ordered Sr adatom which is located at the oxygen fourfold site on the TiO_2 terminated layer. We theoretically simulated STM and NC-AFM images with the first-principles total-energy calculation and showed that agreement with experimental results was fairly good. The Sr adatom causes less distortion in the bulk, compared with the TiO_2 terminated 1×1 model. The wave functions near the Fermi level are localized at the Sr adatom and their shape and size are consistent with our STM results.

This work was supported in part by Grants-in-Aid from the Science and Technology Agency.

*Corresponding author.
Email address: nozoye@nimc.go.jp

[1] V. E. Henrich and P. A. Cox, *The Surface Science of Metal Oxides* (Cambridge University Press, Cambridge, U.K., 1994).
[2] M. Bäumer and H.-J. Freund, Prog. Surf. Sci. **61**, 127 (1999).
[3] C. N. R. Rao and B. Raveau, *Transition Metal Oxides* (VCH, New York, 1995).
[4] J. Tersoff and D. R. Hamann, Phys. Rev. B **31**, 805 (1985).
[5] F. J. Giessibl, Science **267**, 68 (1995).
[6] H. Ueyama *et al.,* Jpn. J. Appl. Phys. **34**, L1086 (1995).
[7] M. Bammerlin *et al.,* Probe Microsc. **1**, 1 (1997).
[8] H. Onishi and Y. Iwasawa, Phys. Rev. Lett. **76**, 791 (1996).
[9] Y. Liang and D. A. Bonnell, Surf. Sci. **285**, L510 (1993).
[10] Q. D. Jiang and J. Zegenhagen, Surf. Sci. **367**, L42 (1996); **425**, 343 (1999).
[11] H. Tanaka *et al.,* Jpn. J. Appl. Phys. **32**, 1405 (1993).
[12] R. Akiyama *et al.,* Jpn. J. Appl. Phys. **36**, 3881 (1997).
[13] S. Kimura *et al.,* Phys. Rev. B **51**, 11 049 (1995).
[14] D.-K. Seo *et al.,* Surf. Sci. **370**, 245 (1997).
[15] M. Kawasaki *et al.,* Science **266**, 1540 (1994).
[16] W. Kohn and L. J. Sham, Phys. Rev. **140**, A1133 (1965).
[17] J. P. Perdew, Physica (Amsterdam) **172B**, 1 (1991).
[18] D. Vanderbilt, Phys. Rev. B **41**, 7892 (1990).
[19] H. J. Monkhorst and J. D. Pack, Phys. Rev. B **13**, 5188 (1976).
[20] K. Yokoyama *et al.,* Phys. Rev. Lett. **83**, 5023 (1999).
[21] M. Ashino *et al.,* Appl. Surf. Sci. **157**, 212 (2000).
[22] T. Minobe *et al.,* Appl. Surf. Sci. **140**, 298 (1999).
[23] Z.-Q. Li *et al.,* Phys. Rev. B **58**, 8075 (1998).
[24] J. Padilla and D. Vanderbilt, Surf. Sci. **418**, 64 (1998).
[25] I. Y. Sokolov *et al.,* Surf. Sci. **381**, L558 (1997); Appl. Surf. Sci. **140**, 362 (1999).